Article

Chinese Science Bulletin

Fluid Mechanics

March 2012 Vol.57 No.8: 849–857
doi: 10.1007/s11434-011-4948-3

Aerodynamic optimization and evaluation for the three-dimensional afterbody/nozzle integrated configuration of hypersonic vehicles

GAO TaiYuan[1], CUI Kai[1*], WANG XiuPing[1], HU ShouChao[1], YANG GuoWei[1] & REN Liang[2]

[1] *Key Laboratory of High Temperature Gas Dynamics, Institute of Mechanics, Chinese Academy of Science, Beijing 100190, China;*
[2] *China Petroleum Pipeline Offshore Engineering, Langfang 065000, China*

Received September 1, 2011; accepted October 27, 2011

The optimization of 2D expansion lines and key parameters of three-dimensional configurations was carried out under simulated conditions of Mach 6.5 and a flight altitude of 25 km for an integrated configuration of the afterbody/nozzle of a hypersonic vehicle. First, the cubic B-spline method was applied to parameterize the expansion lines of the upper expansion ramp. The optimization procedure was established based on computational fluid dynamics and the sequential quadratic programming method. The local mesh reconstruction technique was applied to improve computational efficiency. A three-dimensional integrated configuration afterbody/nozzle was designed based on the two-dimensional optimized expansion lines. The influence rules incorporated certain key design parameters affecting the lift and thrust performance of the configuration, such as the ratio of the lengths of the lower expansion ramp to the afterbody (l/L), the dip angle of the lower expansion ramp ω, and the ratio of exit height to the length of afterbody (H/L). Under these conditions, we found that the integrated configuration has optimal performance when l/L=1/6, H/L=0.35 and ω=10°. We also showed that the presence of a side-board promotes lift and thrust performance, and effectively prevents the leakage of high pressure gas.

hypersonic, afterbody/nozzle integrated configuration, single expanding ramp nozzle, optimization, computational fluid dynamics

Citation: Gao T Y, Cui K, Wang X P, et al. Aerodynamic optimization and evaluation for the three-dimensional afterbody/nozzle integrated configuration of hypersonic vehicles. Chin Sci Bull, 2012, 57: 849–857, doi: 10.1007/s11434-011-4948-3

For scramjet-powered hypersonic vehicles, an integrated configuration body/engine design is usually adopted. The wave rider or lift body configuration is used as the fore body. Therefore the fore body of hypersonic vehicle provides most of the lift and also forms the pre-compression face of the engine inlet. The afterbody of the vehicle can be considered as an extension to the nozzle, providing lift and thrust. With this design, the bottom surface of the airframe is fully integrated with the propulsion system, and therefore drag force can be reduced. As a result, the afterbody of vehicle is designed as an integrated structure with the engine nozzle. The afterbody is the major thrust producing component, providing more than 50% of the total engine thrust [1,2].

The single expansion ramp nozzle is a typical propulsion system design. For a given Mach number, attack angle and dynamic pressure, the airflow expansion and the aerodynamic performance of afterbody mainly depend on its geometry, especially the upper expansion line. Early methods of nozzle design adopted the characteristic and the variational method to achieve the maximum lift-drag ratio or minimum length of nozzle based on inviscid flow theory (typically Rao's method) [3,4]. The flow phenomena in the entry (i.e. the engine and afterbody exhausts) of nozzle are very complex, so nozzle designs based on inviscid flow theory are generally only regarded as preliminary [4]. In recent years, with the development of computational fluid dynamics (CFD), high credibility numerical simulation has become the main analytical tool for performance evaluation [5–7], design [8,9] and particularly optimization [2,10–15]

*Corresponding author (email: kcui@imech.ac.cn)

of hypersonic vehicle nozzles. For example, Chen et al. [2,10] used the cubic B-spline method to parameterize the upper expansion line of a nozzle, and a nonlinear simplex method to optimize a two-dimensional nozzle. Based on a large number of numerical experiments, Marathe et al. [11,12] optimized a nozzle with a response surface constructed using the latin square technique. He et al. [13] and Che et al. [14] optimized a two-dimensional integrated configuration afterbody/nozzle using the genetic method, and CFD analysis; both methods achieved very significant results.

For a hypersonic vehicle, optimizing the three-dimensional integrated configuration afterbody/nozzle directly by numerical analysis and optimization methods is a more reasonable option, but under three-dimensional conditions, the flow phenomena of the afterbody is very complex, and the optimization involves a large number of design variables, and consequently needs a large amount of computing resources and computing time. However, extending the optimized two-dimensional expansion line to a three-dimensional expansion nozzle can avoid these problems. Current research on the integrated configuration afterbody/nozzle is mainly focused on the optimization of the two-dimensional expansion line. However, with a single expansion ramp nozzle design under three-dimensional conditions, the internal and external nozzle flows mix directly in the expansion region. The high pressure gas will leak to both sides of the nozzle, and the flow fields will significantly differ from the two-dimensional case. Clearly, the performance of a three-dimensional expansion nozzle may not be accurately predicted from the optimized two-dimensional expansion line.

Therefore, we have undertaken three design condition exercises working at Mach 6.5 and a flight altitude of 25 km. First, for the two-dimensional integrated configuration afterbody/nozzle, the cubic B-spline method was applied to parameterize the expansion line, and the line was optimized by CFD analysis and numerical optimization to achieve the maximum lift-drag ratio. The multi-block structured grids were generated as a computational mesh. The local mesh reconstructed technique was applied to improve computational efficiency. This technique aims to ensure the quality of the mesh and the precision of the results. Second, building on the two-dimensional optimization exercise, a three-dimensional integrated configuration afterbody/nozzle was designed by CFD. The three-dimensional effects on aerodynamic performance were analyzed. Finally, for a three-dimensional configuration, the influence rules incorporated certain key design parameters affecting the lift and thrust performance of the configuration, such as the ratio of the lengths of the lower expansion ramp to the afterbody (l/L), the dip angle of the lower expansion ramp ω, the ratio of exit height to the length of afterbody (H/L). In addition the influence of the side-board on the aerodynamic performances of the configuration was determined.

The results show that the optimization of two-dimensional configuration is also effective under three-dimensional conditions. However, the aerodynamic performance of the initial and optimized three-dimensional configuration is worse than the two-dimensional configuration. Therefore the three-dimensional effect cannot be neglected. The results show the three-dimensional integrated configuration has the best overall performance with l/L=1/6, H/L=0.35 and ω=10°. We have also shown that the presence of a side-board promotes lift and thrust performance, and effectively prevents the leakage of high pressure gas

1 The optimization for the expansion line of two-dimensional integrated configuration afterbody/nozzle

1.1 The parametric method for the two-dimensional expansion line

We used the cubic B-Spline method to parameterize the upper expansion line of two-dimensional configuration [16]. The equation is

$$P(t)=\frac{1}{6}\begin{bmatrix}t^3 & t^2 & t & 1\end{bmatrix}\begin{bmatrix}-1 & 3 & -3 & 1\\ 3 & -6 & 3 & 0\\ -3 & 0 & 3 & 0\\ 1 & 4 & 1 & 0\end{bmatrix}\begin{bmatrix}P_0\\ P_1\\ P_2\\ P_3\end{bmatrix},t\in[0,1]. \quad (1)$$

$P(t)=(x(t), y(t))$ indicates the upper expansion line, P_0–P_3 indicates the coordinates of the control points, $P_i=(x_i,y_i)$. Four points (eight parameters) were used to parameterize the expansion line, as shown in Figure 1.

Point 1 is the junction point between the afterbody and the engine exit, which is a fixed point determined by the shape of the engine and the installation position. Point 4 is the tail end of the afterbody. The X-coordinate of point 4 is determined by the length of the airframe and the afterbody,

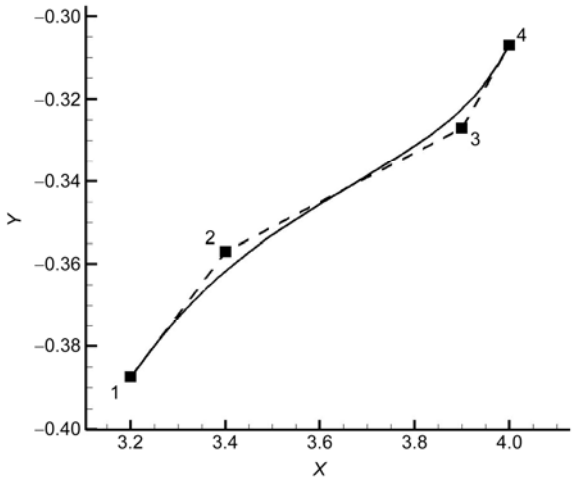

Figure 1 An example of afterbody parameterization.

and the *Y*-coordinate as an adjustable point but not a design variable, is determined by the exit height of the afterbody. The *X* and *Y* coordinates of points 2 and 3 are the four design variables.

1.2 The CFD analysis method and the local mesh reconstruction technique

Three-dimensional Reynolds-averaged Navier-Stokes equations are used to compute the flow fields. The implicit lower-upper Symmetric-Gauss-Seidel (LU-SGS) method with sub-iteration is used for time marching, which can improve computational stability. The sub-iteration can eliminate numerical errors caused by nonlinear equations and the hysteretic boundary conditions. The improved Harten-Lax-van Leer-Einfeldt-Wada (HLLEW) scheme is used for the spatial discretization which can improve computing accuracy. The scheme returns to the upwind Roe scheme in the isentropic flow region, and changes to a HLLE scheme in flow regions with large entropy changes. Therefore the scheme can overcome the non-physical oscillations generated in the process of simulating the shock wave flow using the Roe scheme. It can also overcome the large numerical viscosity generated in the process of simulating continuous flow using the HLLE scheme. The central difference method is used to discretize the viscosity term, and the k-ε model is used to simulate turbulence. The lift coefficient and the thrust coefficient are computed from the expansion ramp of the integrated configuration afterbody/nozzle. The pressure distributions on the expansion ramp are calculated by CFD analysis. After integration and decomposition in the *X* and *Y* directions, and non-dimensionalization, the lift coefficient and thrust coefficient can be calculated.

In the process of optimization, the computational domains will vary from expansion line to line. To ensure the efficiency and stability of the optimization, the local mesh reconstruction technique is used. The mesh block which directly links to the expansion line, as No. 1 block shown in Figure 2, is a variable block. The rest of the grids stay the same during the process of optimization. No. 1 block will reconstruct constantly as the expansion line changes. This technique has the following three advantages:

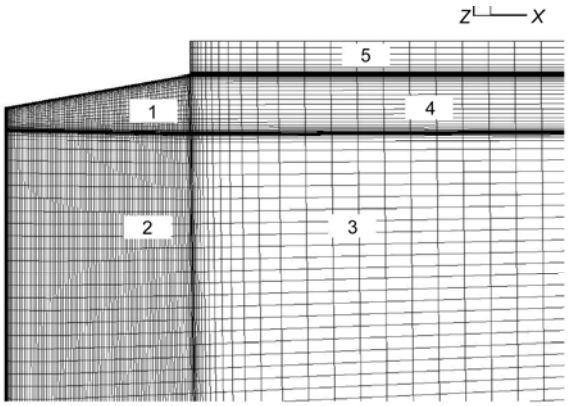

Figure 2 Multi-block grids.

(1) The high-quality mesh will not change after generation, and this will reduce the numerical error caused by the global mesh deformation;

(2) In the process of optimization, only the local mesh needs reconstruction and this can reduce computing time;

(3) In the process of optimization, CFD calculations can proceed based on the results obtained in the previous iteration, so that this technique can also effectively reduce the CFD analysis time.

1.3 Optimization procedure and the optimization method

The overall procedure of optimal design is shown in Figure 3. During the optimization iterations, CFD analysis for the initial shape is the first step to obtain the aerodynamic parameters, then the design variables are adjusted under the direction of the optimization method, the new shape will be generated, and the local mesh will be reconstructed for the CFD analysis of next cycle. This iteration will not stop until the shape and the objective value do not change.

The sequential quadratic programming (SQP) method is used. This method transforms the optimization problem into a series of quadratic programming sub-problems to solve by iterative methods. The SQP method is one of the most stable methods for solving nonlinear optimization problems

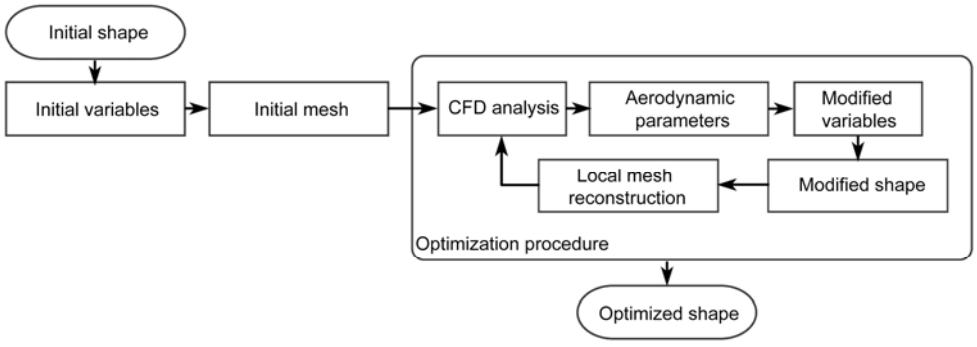

Figure 3 Flowchart of the optimization iteration.

and is a commonly used method for solving small and medium scale practical optimization problems. In the problem under consideration, the gradients of the objective function to design variables are calculated by the numerical differential method, and the Hessian matrix is calculated using the Broyden-Fletcher-Goldfarb-Shanno (BFGS) quasi-Newton method.

1.4 Two-dimensional optimization and the results

To verify the validity of the optimization procedure and obtain the optimal shape, the optimization was first carried out for the expansion line of the two-dimensional integrated configuration afterbody/nozzle to achieve maximum thrust. The lower expansion ramp was not installed on the two-dimensional configuration. The initial exit height to length of afterbody ratio is 0.35, and the initial line is a straight. The other relevant design conditions are shown in Table 1, typical conditions are used for the inlet, and the outlet conditions are obtained by extrapolation.

The compression between the initial and the optimized expansion lines are shown in Figure 4, the compression between initial and optimized aerodynamic coefficients are given in Table 2.

In Table 2, *Ct* represents the thrust coefficient, *Cl* represents the lift coefficient, while ΔCt and ΔCl represent the increment of thrust coefficient and lift coefficient after optimization, which is defined by $\Delta = \dfrac{\text{optm} - \text{init}}{\text{init}} \times 100\%$. Initial-2D and Optimized-2D represent the two-dimensional initial shape and optimized shape.

As shown in Table 2, the thrust coefficient increased after optimization, but in contrast, the lift coefficient had a relatively small reduction. The difference between the pressure contours of the local flow field is given in Figure 5. It can be seen that for the initial configuration, the pressure coefficient at the expansion ramp is higher in the front of the afterbody, but reduces dramatically to the rear. For the optimized configuration, the ejected gas fully expands. The pressure is higher along the expansion ramp. This is the main reason for improvement in the thrust.

Table 1 Computational condition for the optimization of afterbody

Ma	α (°)	P_∞ (Pa)	T_∞ (K)
6.5	0	2550	221.6

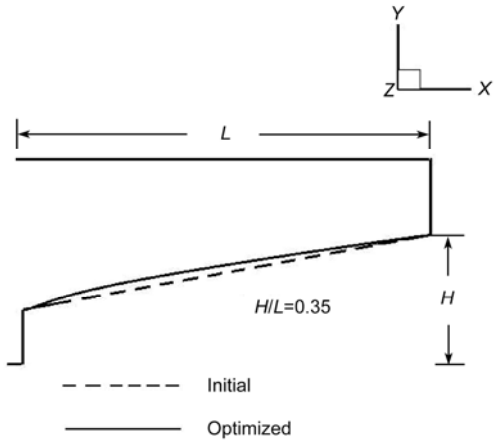

Figure 4 Comparison between initial and optimized profiles of the afterbody.

Table 2 Aerodynamic coefficients comparison between the 2D initial and optimized shapes

	Ct	ΔCt	*Cl*	ΔCl
Initial-2D	0.0247	4.45%	0.1319	1.90%
Optimized-2D	0.0258		0.1294	

2 The three-dimensional effect

To examine the impact of the three-dimensional effect, a three-dimensional integrated configuration afterbody/nozzle was designed, based on the two-dimensional optimization. The

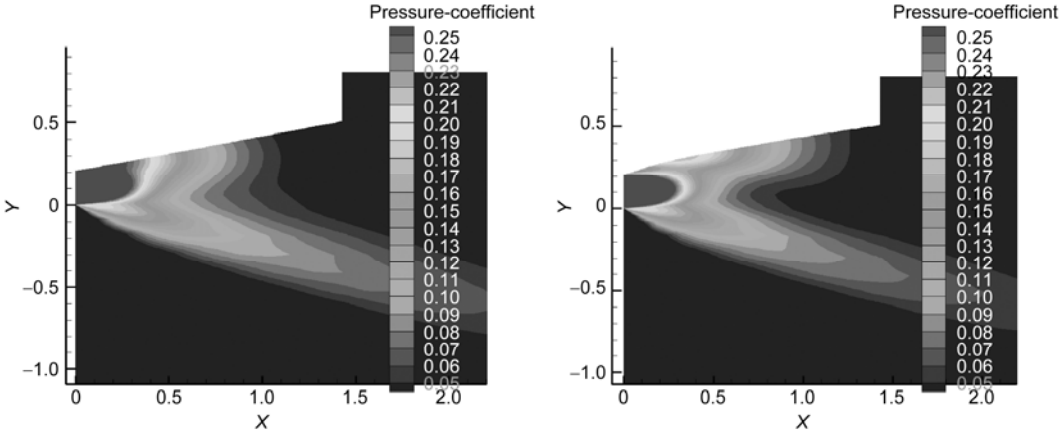

Figure 5 Pressure contours of local field around the afterbody.

design approach is as follows: making a lateral extension from the two-dimensional expansion line and a rectangular section of afterbody along axial direction. The aspect ratio for the entrance of the afterbody is 3.1, the aspect ratio for the exit of afterbody is 2 and the area ratio of exit to entrance is 3.663. Based on the two-dimensional expansion line, an initial and optimized three-dimensional configuration were designed, and computed by CFD. The aerodynamic coefficients are listed in Table 3. The pressure distributions on the expansion ramp along the x axis under two and three-dimensional condition are given in Figure 6.

Initial-3D and Optimized-3D represent the two-dimensional initial shape and optimized shape respectively in Table 3. The other parameters are the same as in Table 2. To ensure the comparability, the reference area under three-dimensional condition is taken as the vertical projection area of the upper expansion ramp.

As shown in Table 3, the thrust coefficient increased after optimization, but in contrast the lift coefficient had a relatively small reduction. This is the same as the results under two-dimensional conditions. The results show that the optimization of the two-dimensional configuration is also effective under three-dimensional conditions. However, both the lift and thrust coefficients under three-dimensional conditions are significantly reduced compared to the results obtained under two-dimensional conditions. From the results shown in Figure 6, for both the initial and optimized shapes, the pressure coefficients of three-dimensional configuration are less than the coefficients of two-dimensional configuration. This shows that the side leakage of high pressure gas has a great impact to the aerodynamic performance. In addition, the pressure of the initial configurations decreases gradually along the x axis, and is lower than the optimized configurations in the rear of the expansion ramp. For the optimized configuration, it can be seen that the pressure distribution of the three-dimensional shape is basically the same as the two-dimensional shape. Both shapes expand better than the initial configuration, and generate a high pressure zone on the upper expansion ramp. The side leakage of the high pressure gas means that the pressure distributions of three-dimensional configuration are less than the two-dimensional configuration, consequently the aerodynamic performance of the afterbody was reduced.

From these three-dimensional configuration results it can be seen that because of the side leakage, the aerodynamic performance of the afterbody declines. Therefore, the aerodynamic performance of three-dimensional configuration extended from the two-dimensional optimized line cannot be guaranteed. For the design of an optimal configuration, it is necessary to consider the three-dimensional effect.

Table 3 Aerodynamic coefficients comparison between the Initial-3D and Optimized-3D afterbody

	Ct	Δ*Ct*	*Cl*	Δ*Cl*
Initial-3D	0.0145	7.59%	0.0796	2.64%
Optimized-3D	0.0156		0.0775	

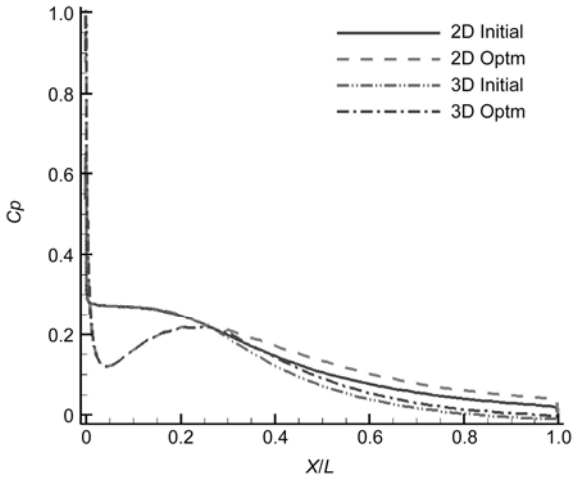

Figure 6 Pressure distributions on the expansion line along the x axis.

3 Three-dimensional afterbody/nozzle configuration and its impact to the aerodynamic performance of the aircraft

3.1 Three-dimensional afterbody/nozzle configuration and design variables

Based on the above results, further analyses for three-dimensional configuration were done based on the two-dimensional optimization. The three-dimensional configuration extended from an optimized expansion line is shown in Figure 7. The lower expansion ramp was installed on the three-dimensional configuration. As shown in Figure 7, L indicates the length of afterbody, l indicates the length of lower expansion ramp, ω indicates the dip angle of the lower expansion ramp and H indicates the exit height. L is unchanged in the process of optimization. Adjusting the geometrical parameters l/L, ω and H/L, quantifies the effect of these parameters to the aerodynamic performance. Here l/L indicates the ratio of the length of the lower expansion ramp to length of the afterbody, and H/L indicates the ratio of exit height to length of afterbody. The width of afterbody is unchanged, so adjusting H/L is equivalent to adjust the ratio of exit to entrance area. l/L was assigned values of 0, 1/6, 1/4, 1/3, ω was assigned values of 7°, 10°, 13° and H/L was assigned values of 0.35, 0.49, 0.63, respectively. All the parameters were given as dimensionless values, and the aerodynamic coefficients were computed from the upper and lower expansion ramp.

The relevant computational conditions and model are the same as the two-dimensional configuration. The computational mesh is a multi-block structured grid, as shown in Figure 8. All the configurations use the same mesh distribution, and

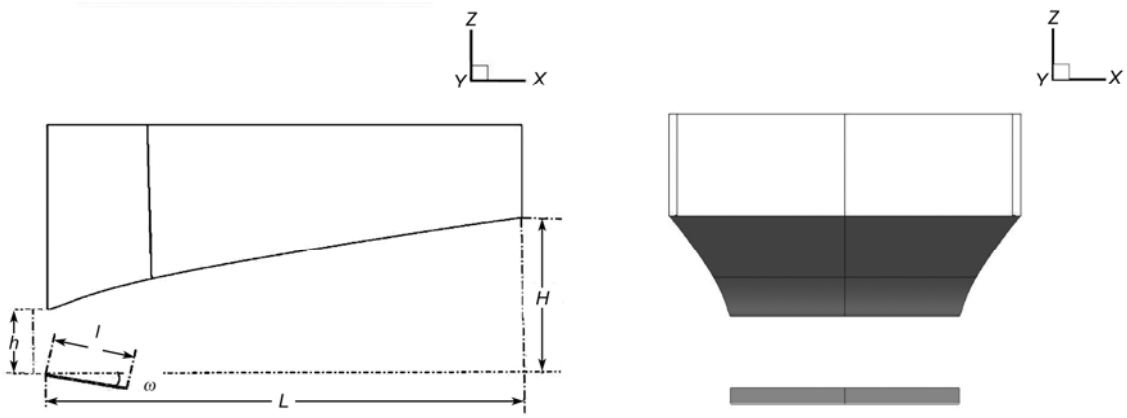

Figure 7 Three-dimensional configuration.

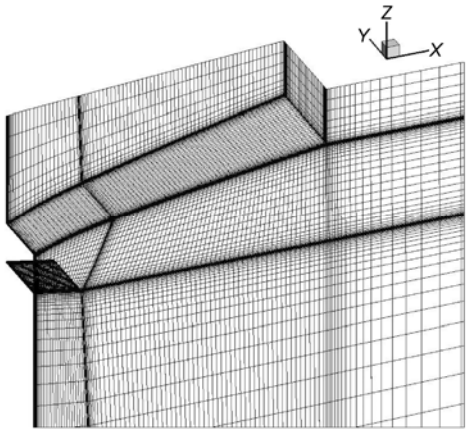

Figure 8 Local zones of the CFD field.

Table 4 Aerodynamic coefficients comparison with different *l*/*L*

l/*L*	*Ct*	*Cl*
0	0.0156	0.0775
1/6	0.0215	0.0430
1/4	0.0234	0.0355
1/3	0.0242	0.0267

the first layer of the boundary layer grid meets $y^+<10$.

3.2 The effect of *l*/*L* on the aerodynamic performance of afterbody

First, the effect of *l*/*L* on the aerodynamic performance of the afterbody was investigated. *l*/*L* refers to the ratio of lengths of the lower expansion ramp to the afterbody. The parameter *H*/*L* was set to 0.35, and ω was set to 7°. The lift coefficient and thrust coefficient computed are shown in Table 4. These coefficients were obtained from the orthogonal decomposition of the pressure on the inner wall of both the upper and lower expansion ramp.

It can be seen from Table 4 that a lower expansion ramp results in an increase of thrust coefficient *Ct*, but a decrease in lift coefficient *Cl*. This is because the increase of *l*/*L* enlarged the force area on the lower expansion ramp. Then the downward leakage of the gas was reduced, which contributes to both the thrust increase, and the lift decrease. The comparison diagram between the aerodynamic parameters *Ct* and *Cl* under different *l*/*L* is shown in Figure 9. As we can see from this figure, the reduction in magnitude of lift is larger than the increase in thrust. For an optimal design, it is necessary to consider the balance of the aerodynamic performances.

3.3 The effect of *H*/*L* on the aerodynamic performance of the afterbody

With the width of the configuration remaining unchanged, adjusting *H*/*L* is equivalent to adjusting the ratio of exit to entrance areas. The parameter *l*/*L* was set to 1/6, and ω was set to 7°. The lift coefficient and thrust coefficient computed are shown in Table 5. The pressure contours on the expansionramps of the afterbody are shown in Figure 10.

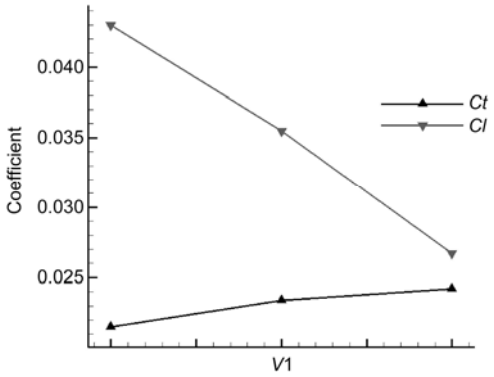

Figure 9 Aerodynamic coefficients comparison with different *l*/*L*.

Table 5 Aerodynamic coefficients comparison with various values of *H*/*L*

H/*L*	*Ct*	*Cl*
0.35	0.0215	0.0430
0.49	0.0195	0.0031
0.63	0.0131	0.0235

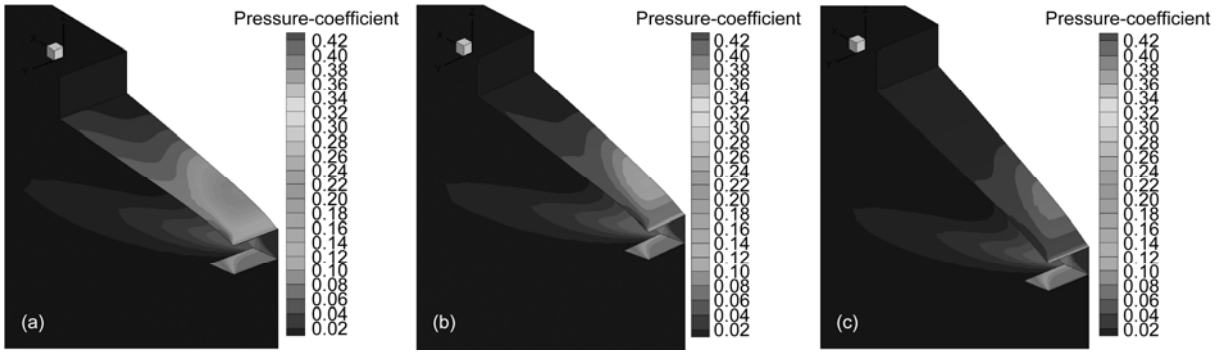

Figure 10 Pressure contours on the expansion ramps of aft bodies with H/L =0.35 (a), 0.49 (b) and 0.63 (c).

It can be seen from Table 5, that the thrust coefficient Ct and lift coefficient Cl decreased as H/L increased. The lift coefficient Cl became negative when H/L was equal to 0.63. The magnitude of the reduction of Cl is larger than the reduction of Ct.

This is because the increase of H/L enlarged the expansion area. Therefore the pressure on the upper expansion ramp was reduced, especially in the rear, and the aerodynamic performance declined. As shown in Figure 10, the pressure distributions on the lower expansion ramp of three configurations are almost the same, but for the upper ramp, the pressure distribution is better when H/L is equal to 0.35. There is no obvious high pressure zone on the upper ramp when H/L is equal to 0.63, so it is better to chose 0.35 for H/L.

3.4 The effect of ω on the aerodynamic performance of the afterbody

After determinations with l/L equal to 1/6 and H/L equal to 0.35, the effect of ω on the aerodynamic performance was further examined. The parameter ω was set to 7°, 10° and 13°, and three configurations were designed. The lift coefficient and thrust coefficient computed are shown in Table 6. The pressure contours on the expansion ramp of the afterbody are given in Figure 11.

It can be seen from Table 6, that Cl and ω are positively correlated. The increase of ω reduced the project area of the lower expansion ramp in the normal direction, so the pressure on the lower expansion ramp was reduced.

However, the thrust coefficient Ct increased and then decreased with an increase in ω. The thrust coefficient achieved a maximum value when $\omega = 10°$. This shows the increase of ω in the range 7° and 13° reduced the project area of the lower expansion ramp in the axial direction and the thrust increased. An over-large dip angle of the lower expansion ramp caused downward leakage of the high pressure gas. The pressure on the lower ramp reduced, and the thrust coefficient declined. In addition, the over-large dip angle ω would enlarge the windward area of the lower expansion ramp, so increase the drag. As shown in Figure 11, the pressure distributions on the upper expansion ramp in all three configurations are almost the same. For the lower ramp, the pressure distribution is the worst when ω= 13°, so it is better to chose 10°.

Through the above analysis on the effects of geometric parameters on the aerodynamic performance, the effect of

Table 6 Aerodynamic coefficients comparison with variation in ω

ω	Ct	Cl
7°	0.0215	0.0430
10°	0.0218	0.0463
13°	0.0217	0.0499

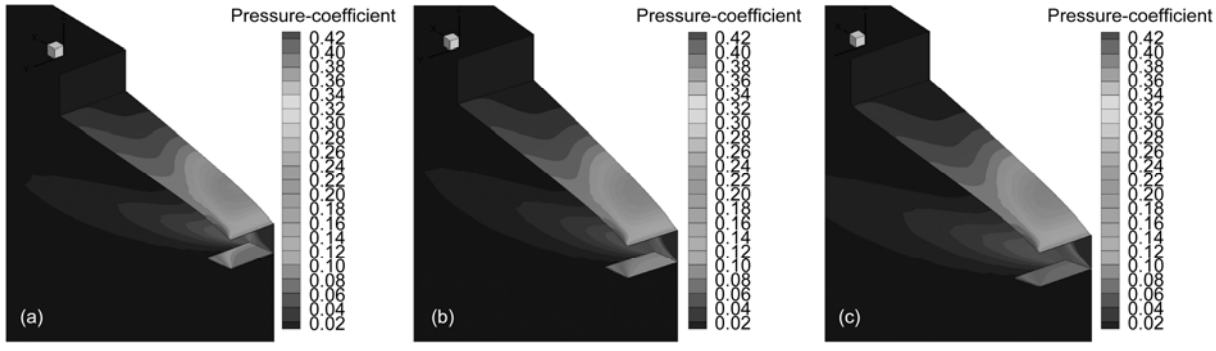

Figure 11 Pressure contours on the expansion ramps of afterbodies with ω=7° (a), 10° (b) and 13° (c).

H/*L* to aerodynamic performance is more significant than that of *l*/*L* and ω. The performance can be improved by appropriately adjusting *H*/*L*. As *l*/*L* is increased, the thrust coefficient *Ct* increases, but the lift coefficient *Cl* rapidly decreases. Therefore a smaller *l*/*L* ratio is recommended. As the variation in range of ω is small, 10° is a better choice. In conclusion, *l*/*L*=1/6, *H*/*L*=0.35 and ω=10° are optimal choices.

It can be seen from Figures 10 and 11 that for the expansion ramps of all six configurations, the pressure near the center is larger than the pressure away from the center line. This shows that there is side leakage of high pressure gas. This is the main reason for the decline of aerodynamic performance. To analyze the effect of this side leakage, an optimized three-dimensional configuration with a side-board was designed, and the effect of the side-board on aerodynamic performance was quantified.

4 The effect of a side-board on the aerodynamic performance of the afterbody

Through the above analysis of the results of the three-dimensional configuration, the performance of the afterbody is better when *l*/*L*=1/6, *H*/*L*=0.35 and ω=10°. Based on the optimized three-dimensional configuration, the effect of a side-board on the afterbody performance was analyzed. The aerodynamic coefficients for afterbodies with and without a side-board were given in Table 7.

In Table 7, *l*/*L*=1/6, *H*/*L*=0.35 and ω=10°. *Ct* represents the thrust coefficient, *Cl* represents the lift coefficient, while ΔCt and ΔCl represent the increment of thrust coefficient and lift coefficient with a side-board, which is defined by $\Delta = \dfrac{\text{with} - \text{without}}{\text{without}} \times 100\%$. With and Without represent the configuration with and without a side-board.

It can be seen from Table 7, that the aerodynamic coefficients increased after the side-board was installed, which is because the side-board prevented the side leakage of high pressure gas. As the pressure on the expansion ramps increased, so the aerodynamic performance of the aircraft improved.

The pressure contours on the expansion ramps for configurations with and without the side-board are given in Figure 12. For the configuration with side-board, there is a high pressure zone on the side-board, and the sidewise leakage of gas was prevented. The pressure distribution on the upper expansion ramp is higher and more uniform. For the configuration without side-board, the upper expansion ramp was not well used, and the pressure away from the center line is lower.

Table 7 Aerodynamic coefficients comparison between aft bodies with and without a sideboard

Sideboard	*Ct*	ΔCt	*Cl*	ΔCl
Without	0.0218	16.51%	0.0463	38.66%
With	0.0254		0.0642	

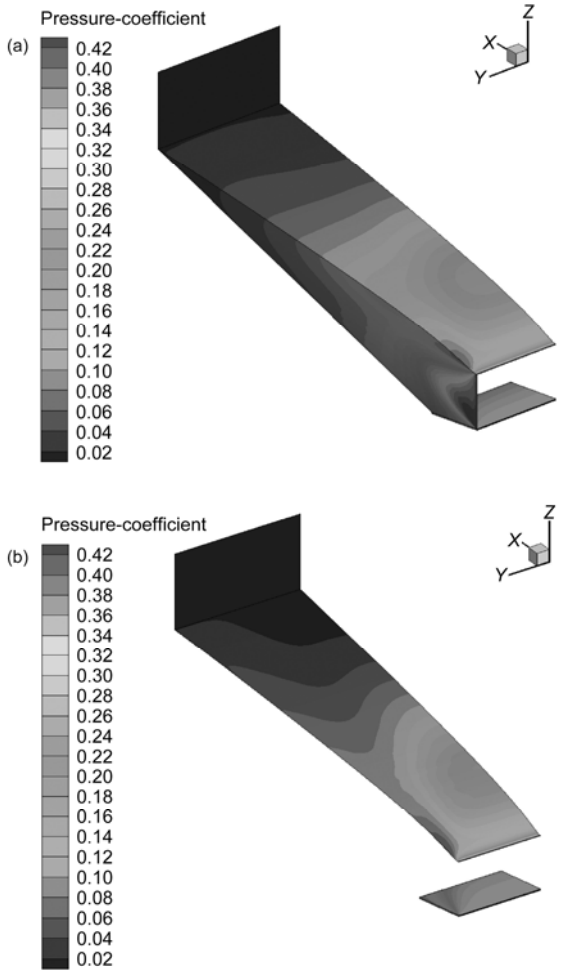

Figure 12 Pressure contours on expansion ramp of afterbodies with (a) and without (b) the sideboard.

The pressure distributions on the upper expansion ramp for these two configurations are given in Figure 13. From these results, the pressure of the configuration without the side-board is less than the configuration with the side-board. Therefore, for an optimal design, a side-board should be installed.

5 Conclusions

CFD analysis was used to predict aerodynamic performance. The SQP method and the B-spline method were applied to establish the optimization procedure for a two-dimensional integrated configuration afterbody/nozzle. The optimization of the expansion line demonstrates the effectiveness of the procedure. Based on these results, the following conclusions can be drawn:

(1) The optimization procedure based on CFD analysis

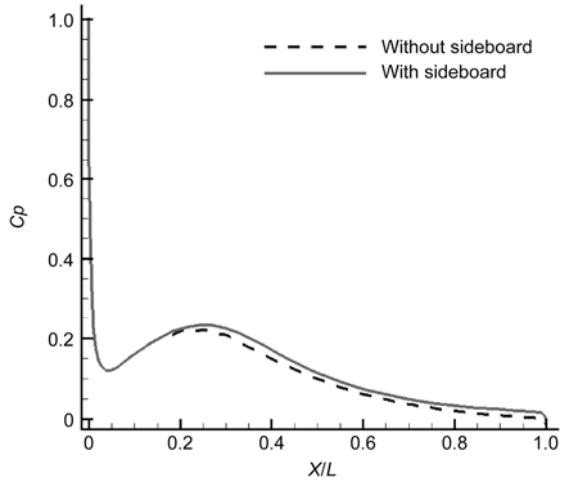

Figure 13 Pressure distributions on the upper expansion line along the *x* axis.

method and local mesh reconstruction technique is effective, and can be applied to the optimization and design of actual aircraft.

(2) The ejected gas fully expanded after optimization, and the thrust coefficient increased significantly, but in contrast, the lift coefficient was slightly reduced.

To examine the impact of the three-dimensional effect, based on a two-dimensional optimization, a three-dimensional integrated configuration afterbody/nozzle was designed. The pressure coefficients of the three-dimensional configuration are less than the coefficients of the equivalent two-dimensional configuration. Therefore, for the design of an optimal configuration, it is necessary to consider the three-dimensional effect. Based on this three-dimensional configuration, by adjusting the geometrical parameters l/L, ω and H/L, further analyses of the three-dimensional configuration were done based on the two-dimensional optimization. Here l/L indicates the ratio of length of the lower expansion ramp to the length of the afterbody, ω indicates the dip angle of the lower expansion ramp and H/L indicates the ratio of exit height to length of afterbody. The following conclusions can be drawn:

(1) Within a certain range, with the increase of l/L, the thrust coefficient Ct increased, and the lift coefficient Cl decreased. For optimal design, it is necessary to consider the balance of the aerodynamic performance.

(2) An increase of H/L would enlarge the expansion area. This reduces the pressure on the upper expansion ramp, more so in the rear, and the aerodynamic performance especially lift, declined.

(3) Within a certain range of ω, the lift coefficient Cl increased with ω, but for the thrust coefficient, there is an optimal dip angle. The thrust performance will decline if the dip angle ω is too large;

(4) Based on all the results, l/L=1/6, H/L=0.35 and ω=10° are the optimal choices;

(5) Installing a side-board can effectively prevent the side leakage of high pressure gas and promote the lift and thrust performance of the aircraft.

This work was supported by the National Natural Science Foundation of China (90916013).

1 Huang Z C. The aerodynamic design for aerospace plane (in Chinese). Aerodyn Exp Meas Control, 1991, 5: 1–11
2 Chen B, Xu X, Cai G B. Optimization design of two dimensional scramjet nozzle based on N-S equations (in Chinese). J Propul Tech, 2002, 23: 433–437
3 Rao G V R. Exhaust nozzle contour for optimum thrust. Jet Propul, 1958, 38: 377–382
4 Huang Z C. The aerodynamic design of nozzle for aerospace plane (in Chinese). Aerodyn Exp Meas Control, 1993, 7: 1–10
5 Berens T M. Experimental and numerical analysis of a two-duct nozzle/afterbody model at supersonic mach numbers. AIAA-1995-6085, 1995
6 Le Bozec A, Rostand P, Rouy F, et al. Afterbody testing and comparison to CFD simulations. AIAA-1998-1596, 1998
7 Zhao J X, Zhou L. Numerical investigation of internal and external supersonic flows of nozzle (in Chinese). J Propul Tech, 2001, 22: 295–298
8 Wang X F, Shang X S, Chen Y C, et al. Numerical simulation of internal flow field in the single expansion ramp nozzle for the hypersonic aero-engine (in Chinese). J Proj Rockets Missiles Guidance, 2007, 27: 187–189
9 Huang W, Liu J, Luo S B. Effect research of afterbody nozzle configuration on hypersonic vehicle performance (in Chinese). J Proj Rockets Missiles Guidance, 2008, 28: 161–164
10 Chen B, Xu X, Cai G B. Single- and multi-objective optimization of scramjet components using genetic algorithms based on a parabolized navier-stokes solver. AIAA-2006-4686, 2006
11 Marathe A G, Thiagarajan V. Effect of geometric parameters on the performance of single expansion ramp nozzle. AIAA-2005-4429, 2005
12 Damira S K, Marathe A G, Sudhakar K. Parametric optimization of single expansion ramp nozzle (SERN). AIAA-2006-5188, 2006
13 He X Z, Zhang Y, Wang G Y, et al. Automated design optimization of single expansion ramp nozzle for hypersonic vehicle (in Chinese). J Propul Tech, 2007, 28: 148–151
14 Che J, Tang S. The application of genetic algorithms to afterbody/nozzle integrated design of a hypersonic vehicle (in Chinese). Flight Dyn, 2006, 24: 74–77
15 Cao D Y, Lee C H. Optimal design of nozzle for hypersonic vehicle (in Chinese). J Beijing Uni Aeronaut Astronaut, 2007, 33: 1162–1165
16 Cui K, Yang G W. The effect of conical flowfields on the performance of waveriders at Mach 6. Chin Sci Bull, 2007, 52: 57–64